Photosensitiser functionalised luminescent upconverting nanoparticles for efficient photodynamic therapy of breast cancer cells

Markus Buchner[a#], Paula García Calavia[b#], Verena Muhr[a], Anna Kröninger[a], Antje Baeumner[a], Thomas Hirsch[a*], David A. Russell[b] and María J. Marín[b*]

[a]Institute of Analytical Chemistry, Chemo- and Biosensors, University of Regensburg, 93040 Regensburg, Germany.

[b]School of Chemistry, University of East Anglia, Norwich Research Park, Norwich, Norfolk, NR4 7TJ, UK.

*Corresponding author at: Institute of Analytical Chemistry, Chemo- and Biosensors, University of Regensburg, 93040 Regensburg, Germany. E-mail address: thomas.hirsch@ur.de; telephone: (+49) 941-943-5712; fax: (+49) 941-943- 4064

*Corresponding author at: School of Chemistry, University of East Anglia, Norwich Research Park, Norwich, Norfolk, NR4 7TJ, UK. E-mail address: M.Marin-Altaba@uea.ac.uk; telephone: (+44) (0)1603 59 1679

[#]MB and PGC have contributed equally to this paper.

Abstract

Photodynamic therapy (PDT) is a well-established treatment of cancer in which cell toxic reactive oxygen species, including singlet oxygen ($^1O_2$), are produced by a photosensitiser drug following irradiation of a specific wavelength. Visible light is commonly used as the excitation source in PDT, although these wavelengths do have limited tissue penetration. In this research, upconverting nanoparticles (UCNPs) functionalised with the photosensitiser Rose Bengal (RB) have been designed and synthesised for PDT of breast cancer cells. The use of UCNPs shifts the required excitation wavelength for the production of $^1O_2$ to near infrared light (NIR) thus allowing deeper tissue penetration. The system was designed to maximise the production of $^1O_2$ *via* efficient Förster resonance energy transfer (FRET) from the UCNPs to the photosensitiser. Highly luminescent NaYF$_4$:Yb,Er,Gd@NaYF$_4$ core-shell UCNPs were synthesised that exhibited two main anti-Stokes emission bands at 541 and 652 nm following 980 nm irradiation. RB was chosen as the photosensitiser since its absorption band overlaps with the green emission of the UCNPs. To achieve efficient energy transfer from the nanoparticles to the photosensitiser, the functionalised UCNPs included a short L-lysine linker to attach the RB to the nanocore yielding RB-lysine functionalised UCNPs. The efficient FRET from the UCNPs to the RB was confirmed by luminescence lifetime measurements. The light emitted by the UCNPs at 541 nm, following excitation at 980 nm, generates the $^1O_2$ *via* the RB. Multi-photon and confocal laser scanning microscopies confirmed the internalisation of the RB-lysine-UCNPs by SK-BR-3 breast cancer cells. Cell viability studies revealed that the RB-lysine-UCNPs induced low dark toxicity in cells prior to PDT treatment. Importantly, following irradiation at 980 nm, high levels of cell death were observed in cells loaded with the RB-lysine-UCNPs. Cell death following PDT treatment was also confirmed using propidium iodide and confocal microscopy. The high drug loading capacity (160 RB/nanoparticle) of the UCNPs, the efficient FRET from the UCNPs to the photosensitiser, the high level of accumulation inside the cells and their PDT cell kill suggest that the RB-lysine-UCNPs are promising for NIR PDT and hence suitable for the treatment of deep-lying cancer tumours.

Keywords:

Introduction

Photodynamic therapy (PDT) is a treatment for cancer that involves the production of reactive oxygen species which leads to cell death. Reactive oxygen species, including singlet oxygen ($^1O_2$), are generated by the activation of a photosensitiser drug with light, typically of visible wavelengths.[1] Particularly effective photosensitisers are hydrophobic in nature, since they can be efficiently internalised by the cells through interaction with the lipid layers of the cell membrane.[2, 3] However, such hydrophobicity restricts the delivery and transportation of the photosensitisers through the body.[2, 4] Another issue with photosensitisers that are activated with visible light is the difficulty to treat deep-lying tumours.[5] Therefore, improvements for the extended use of PDT in the clinical environment include the development of photosensitiser delivery systems that can provide aqueous solubility, as well as the use of excitation wavelengths in the near-infrared (NIR) region that can increase tissue penetration.

Upconverting nanoparticles (UCNPs) have attracted considerable interest as delivery vehicles for photodynamic therapy.[5] UCNPs convert NIR light to ultraviolet (UV) and visible light, which can then be used for the excitation of photosensitisers placed near the surface of the UCNPs.[5] The use of NIR light has several advantages over UV and visible light, including deeper penetration into biological tissue, reduced photodamage upon long-term irradiation, increased photostability and low autofluorescence.[5-8] UCNPs are commonly prepared with lanthanide ions, which are embedded in a crystalline host lattice.[9] Such a host lattice is physically and chemically stable and requires low phonon energies,[10] so that non-radiative loss can be minimised while the upconverted emission is maximised.[7, 9, 11] The lanthanide dopants typically consist of ytterbium (Yb^{3+}) ions as sensitiser ions, which can absorb the NIR light and transfer two or more photons to the so-called emitting ions (e.g. erbium (Er^{3+}), holmium (Ho^{3+}) and thulium (Tm^{3+}) ions), yielding anti-Stokes emissions.[7, 9, 11]

Thermolysis, Ostwald ripening and a hydrothermal strategy are the three main synthetic methods for UCNPs.[6] Depending on the performed synthesis, several surface modifications are necessary either to enhance the colloidal stability of the nanoparticles or to provide functional groups on the surface of the particles for coupling with other ligands such as biomolecules and/or photosensitisers.[6, 12, 13] The most important consideration when using UCNPs for PDT is the overlap between the luminescence emission of the UCNPs and the absorption of the photosensitiser, enabling an activation of the photosensitiser by the NIR light.[5] Therefore, the surface modification and functionalisation of the UCNPs with the photosensitiser is critical to achieve efficient photodynamic therapy.[14] Several surface modifications and functionalisation methods have been explored. The first reports of UCNPs for PDT involved the coating of the UCNPs with an amorphous silica layer, to which the photosensitiser was

embedded.[15, 16] Despite the promising results obtained, the silica coating was found to present various limitations, including the low loading of the photosensitiser due to its weak interaction with the silica, the low stability of silica in aqueous solutions and the restricted site of action of singlet oxygen, which is unable to be efficiently released from the silica layer.[17, 18] These limitations could be improved by covalent conjugation of the photosensitiser to the silica layer,[17] or by the use of mesoporous silica ($mSiO_2$), which further improves the aqueous solubility of the system and increases the PDT efficacy due to an improved release of $^1O_2$.[18, 19] The addition of an extra outer layer made of a cross-linked lipid to the $mSiO_2$-UCNPs is a further advantage to avoid the leaking of the photosensitiser from the silica layer.[20]

The use of hydrophilic and amphiphilic polymers have also been widely studied. Polyethylene glycol (PEG) is one such polymer that can induce water solubility and biocompatibility with good results in NIR-PDT, either used by itself,[21] or as a copolymer.[22-24] The addition of PEG has also been reported to increase the stability in a system where the photosensitiser was deposited as a layer around the UCNPs.[25] An additional advantage of PEG is its use as a linker for targeting molecules, such as folic acid.[26] Other polymers that have been used to modify the surface of UCNPs in PDT include polyethyleneimide,[27] chitosan,[28, 29] and a polymeric liposome made of three amphiphilic polymers.[30] The modification of oleate-capped UCNPs with a cyclic oligosaccharide, α-cyclodextrin, yielded water stable and biocompatible UCNPs useful for PDT.[31] A new synthetic approach applying nucleotides to render water dispersible UCNPs without the need of ligand exchange surface modification has been reported by Zhou *et al.*.[32]

A significant problem with the current functionalisation methods is the increase in the distance between the emitting ions in the UCNPs and the photosensitisers, due to the inclusion of the extra layer of either silica or polymers between the two.[33] The distance between the surface of the UCNPs and the photosensitiser needs to be considered as an important parameter, since the energy transfer efficiency is distance-dependent; it decreases proportionally to the sixth power of the distance between the donor and the acceptor species.[33, 34] As a result, the efficiency of $^1O_2$ production and thus photodynamic therapy is reduced.

Here, we report the synthesis of a novel nanoplatform that includes small and bright UCNPs modified with a short biocompatible linker molecule, L-lysine, to which the photosensitiser Rose Bengal (RB) was covalently attached (**Fig. 1**). The nanoparticles exhibit structural advantages including: 1) high drug loading on the surface of the nanoparticles; 2) short distance between the nanoparticle and the photosensitiser; and 3) colloidal stability. The Rose Bengal (RB)-lysine functionalised UCNPs generated singlet oxygen *via* efficient Förster resonance energy transfer (FRET) between the UCNP and the photosensitiser. The use of the UCNPs for photodynamic therapy of cancer was investigated *in vitro* using SK-BR-3 human breast cancer cells. The RB-lysine functionalised UCNPs were internalised by the SK-BR-3 cells as demonstrated using confocal laser scanning microscopy and multi-photon microscopy. Furthermore, cell viability and cytotoxicity studies performed before and after PDT treatment confirmed the high efficiency of the RB-lysine functionalised UCNPs for PDT of cancer.
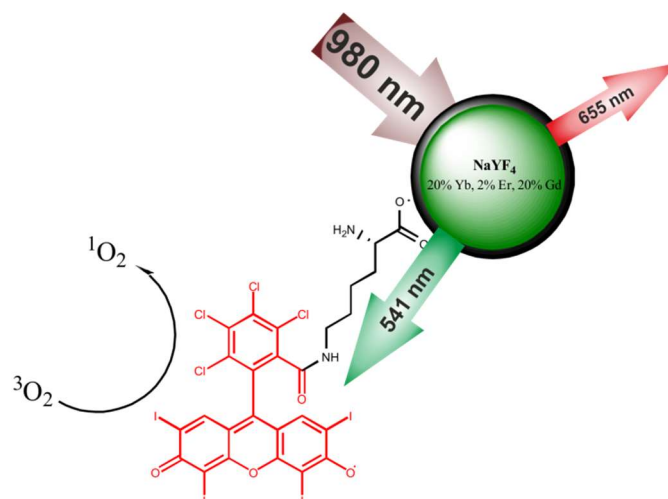

Fig. 1. Schematic representation of the Rose Bengal – lysine functionalised UCNPs used for photodynamic therapy of breast cancer cells. The UCNPs (green) were excited at 980 nm to produce luminescence emission at 541 nm that excited the Rose Bengal (red molecule) to produce singlet oxygen ($^1O_2$), toxic for the cancer cells.

Experimental Section

Materials

All of the reagents used were of analytical grade, purchased from Sigma-Aldrich, unless otherwise stated, and used as received. Sodium dihydrogen orthophosphate dihydrate ($NaH_2PO_4 \cdot 2H_2O$), sodium chloride (NaCl), phosphate buffered saline (PBS) tablets, foetal bovine serum, 75 cm² Nunc Easy tissue

culture flasks with porous caps, Nunc multidishes, Nunc Nunclon™ Δ Surface 96-well white-bottom microplates and 18 mm diameter glass coverslips were purchased from Thermo Fisher Scientific, UK. Trypsin 0.25% (1x) with ethylenediaminetetraacetic acid (EDTA) and McCOY's 5A phenol red free medium containing L-glutamine were purchased from Invitrogen, UK. CellTiter-Blue® cell viability assay was purchased from Promega, UK. Millex GP syringe driven filter units (0.22 μm) were purchased from Millipore Corporation, USA. Sodium hydrogen carbonate ($NaHCO_3$) was purchased from BDH Laboratory Supplies Poole, UK. 1-Octadecene (90%) and oleic acid (90%) were bought from Alfar Aesar. Sodium hydroxide (98-100%) and dimethyl sulfoxide (DMSO, 99.9%) were purchased from Merck. Cyclohexane (99.5%), dimethylformamide (DMF, 99.5%), and chloroform (99.8%) were obtained from Acros Organics. Yttrium chloride hexahydrate (99.99%), ytterbium chloride hexahydrate (99.99%) and gadolinium chloride hexahydrate (99.99%) were bought from Treibacher Industrie AG. L-lysine (98.5-101.5%) was purchased from SERVA. SK-BR-3 human breast adenocarcinoma cells were purchased from LGC Standards. The SK-BR-3 cell line was kindly provided by Prof Dylan R. Edwards (Norwich Medical School, University of East Anglia, UK).

Instrumental

The size of the nanoparticles was investigated with dynamic light scattering (DLS) and transmission electron microscopy (TEM). DLS-measurements were performed on a Zetasizer Nano ZS (Malvern) in semi-micro disposable poly(methyl methacrylate) (PMMA) cuvettes. For particles dispersed in DMF and DMSO, precision cells made of quartz glass Suprasil from Hellma were used. A 120 kV Philips CM12 microscope (MicroCal) was used to generate TEM images, which were analysed with ImageJ/Origin 8. Lifetime measurements were performed with a 980 nm (cw, 200 mW) laser module and an optical chopper (MC2000 with a two-slot chopper blade MC1F2) from Thorlabs. The signal was amplified by a photomultiplier tube and analysed by a digital storage oscilloscope (DSO 8204) from Voltcraft. Optical bandpass filters (FF01-535/150-25 and FF01-665/150-25) from Semrock were used to measure luminescence decay times for the green (541 nm) and the red emission (656 nm). Fourier transform infrared spectroscopy (FTIR) measurements were performed on a Carry 630 FTIR spectrometer (Agilent Technologies). The luminescence spectra were recorded on a luminescence Aminco Bowman Series 2 spectrometer (Thermo Electron Corporation) coupled with a cw laser (980 nm, 200 mW). Inductively coupled plasma optical emission spectrometric (ICP-OES) measurements were performed using an ICP-OES from Spectro.

Multi-photon microscopy was achieved using a TriM Scope II multi-photon microscope (LaVision BioTec, Bielefeld, Germany). The images were acquired with a 63x/1.4 NA PlanApochromat objective

lens (Carl Zeiss Ltd., Cambridge, UK) and processed using ImspectorPro and ImageJ/Fiji software. Laser scanning confocal microscopy images of SK-BR-3 cells were obtained using a Carl Zeiss LSM 510 META microscope. The images were acquired with a plan-apochromat 63x/1.4 Oil DIC objective and processed using the Zeiss LSM Image Browser software. To perform the cell viability assays, the samples were excited at 561 nm and the fluorescence emission was measured at 594 nm using a CLARIOstar® (BMG Labtech) microplate reader.

Methods

Synthesis, functionalisation and characterisation of UCNPs

Synthesis of oleate-capped UCNPs

The synthesis of β-NaYF$_4$:Yb,Er,Gd core, α-NaYF$_4$ shell precursor and NaYF$_4$:Yb,Er,Gd@NaYF$_4$ core-shell (oleate-capped) upconverting nanoparticles has been previously reported[35] and is described in the supplementary information.

Synthesis of BF$_4^-$ capped NaYF$_4$:Yb,Er,Gd@NaYF$_4$ core-shell nanoparticles

For the preparation of BF$_4^-$ capped core-shell nanoparticles, a ligand exchange method was used. Equal volumes of cyclohexane, containing the oleate capped upconverting nanoparticles and DMF were stirred at 30 °C. Nitrosyltetrafluoroborate (NOBF$_4$) was added directly into the stirring solution (1 mg NOBF$_4$ for 1 mg nanoparticles). After 15 min of stirring at 30 °C, the upper phase (cyclohexane) was removed and the DMF phase was washed with an excess of chloroform (20 mL). After being centrifuged (1,000 xg, 5 min), the jelly-like precipitate was dispersed in 2-3 mL DMF and washed with chloroform (20 mL). Finally, the BF$_4^-$ capped nanoparticles were dispersed in 2-3 mL of DMF and the aggregates were separated by centrifugation (1,000 xg, 3 min).

Synthesis of L-lysine functionalised NaYF$_4$:Yb,Er,Gd@NaYF$_4$ core-shell nanoparticles

6 mg L-lysine was dissolved in 2 mL doubly distilled water and was heated to 30 °C. 20 mg of BF$_4^-$ capped core-shell nanoparticles was added to the solution and the dispersion was stirred for 15 min. The particles were centrifuged twice (21,000 xg, 30 min) and redispersed in 2 mL of doubly distilled water under sonication.

Synthesis of Rose Bengal (RB)-lysine functionalised NaYF$_4$:Yb,Er,Gd@NaYF$_4$ core-shell nanoparticles

8 mg Rose Bengal (RB, 8 μmol) was activated with 10 mg of N-(3-dimethylaminopropyl)-N'-ethylcarbodiimide hydrochloride (EDC, 50 μmol) and 10 mg of N-hydroxysuccinimide ester (NHS ester (87 μmol) in 2 mL of 2-(N-morpholino)ethanesulfonic acid (MES, pH 5.5, 50 mM) buffer for 2 h at room temperature. 20 mg of L-lysine functionalised NaYF$_4$:Yb,Er,Gd@NaYF$_4$ core-shell upconverting nanoparticles were added and stirred for a further 2 h. The RB-lysine functionalised NaYF$_4$:Yb,Er,Gd@NaYF$_4$ core-shell nanoparticles were purified *via* centrifugation (21,000 xg, 30 min) three times until the supernatant was clear. The nanoparticles were dispersed in 4 mL DMSO.

Estimation of the concentration of photosensitiser Rose Bengal on the UCNPs

The photosensitiser loading on the RB-lysine functionalised NaYF$_4$:Yb,Er,Gd@NaYF$_4$ core-shell upconverting nanoparticles was estimated using UV-Vis absorption spectroscopy (ε_{RB} = 90,400 M^{-1}·cm^{-1}). The number of the Rose Bengal molecules was divided by the number of nanoparticles calculated by ICP-OES measurements and the density of NaYF$_4$ (3.87 g·cm^{-3}).[36]

Monitoring of singlet oxygen production

The generation of singlet oxygen was monitored with 9,10-anthracenediyl-bis(methylene)dimalonic acid (ABMA, 1 μM), a molecular probe for singlet oxygen. The mass concentration of the nanoparticles was 0.55 mg·mL^{-1} dispersed in either DMSO or in McCOY's 5A phenol red free cell culture medium. The nanoparticles were mixed with ABMA and the solution was placed in a stoppered quartz cuvette. The sample was irradiated with a 980 nm NIR laser (200 mW, Picotronic) for 40 min. The fluorescence emission intensity of ABMA was monitored every 5 min between 390 – 550 nm (λ_{exc} = 380 nm).

<u>*Biological experiments*</u>

A detailed description of the imaging medium, phosphate buffer saline and propidium iodide solution used to perform the biological studies can be found in the supporting information. The protocols used to culture the SK-BR-3 cells and to prepare the coverslips to be used with the confocal laser scanning microscope and the multi-photon microscope are also reported in the supporting information.

Treatment of SK-BR-3 cells to study cellular internalisation of the RB-lysine functionalised NaYF$_4$:Yb,Er,Gd@NaYF$_4$ core-shell UCNPs

The SK-BR-3 cells on the coverslip were washed once with PBS (1 mL). For cells treated with the RB-lysine functionalised NaYF$_4$:Yb,Er,Gd@NaYF$_4$ core-shell UCNPs, a solution of the functionalised UCNPs (1 mL, 25 µg·mL^{-1}) in McCOY's 5A phenol red free medium containing 0.25% DMSO was added to the coverslip. For control cells, 1 mL of McCOY's 5A phenol red free medium was added to the coverslip. The cells were incubated for 3 h at 37 °C in a 5% CO$_2$ atmosphere. Following incubation, the cells were washed three times with PBS (1 mL) and kept in McCOY's 5A phenol red free medium supplemented with 10% foetal bovine serum (2 mL). Subsequently, the cells were imaged using multi-photon and laser scanning confocal microscopes.

Treatment of SK-BR-3 cells to evaluate the PDT effect

The SK-BR-3 cells on the coverslip were washed once with PBS (1 mL). For cells treated with the RB-lysine functionalised NaYF$_4$:Yb,Er,Gd@NaYF$_4$ core-shell UCNPs, a solution of the functionalised UCNPs (1 mL, 15 µg·mL^{-1}) in McCOY's 5A phenol red free medium containing 0.25% DMSO was added to the coverslip. For control cells, 1 mL of the McCOY's 5A phenol red free medium containing 0.25% DMSO was added to the coverslip. The cells were incubated for 3 h at 37 °C in a 5% CO$_2$ atmosphere. Following incubation, the cells were washed three times with PBS (1 mL) and kept in McCOY's 5A phenol red free medium supplemented with 10% foetal bovine serum (2 mL). The 'irradiated cells' were irradiated for 6 min per coverslip using a 980 nm near infrared (NIR) laser (200 mW, Picotronic) placed 50 mm above the lid of the 6-well Nunc multidish. A NIR detector card was placed under the well containing the coverslip during the irradiation of the sample to ensure that the laser light was at the centre of the treated coverslip. Both the irradiated and the non-irradiated SK-BR-3 cells were further incubated at 37 °C in a 5% CO$_2$ atmosphere for *ca.* 24 h until the sample was imaged using a laser scanning confocal microscope.

Imaging of treated SK-BR-3 cells using a multi-photon microscope

For imaging, 18 mm coverslips containing the SK-BR-3 cells of interest were placed in a Ludin chamber, which was securely tightened. Each coverslip was washed three times with HBSS-based imaging medium and the Ludin chamber was mounted on a heated stage at 37 °C in a TriM Scope II multi-photon microscope. The samples were excited with an 880 nm laser using a Vision II Ti: Sapphire laser (Coherent Ltd., Ely, UK) to collect the emission of the RB (green channel, 550 ± 42.5 nm) and the differential interference contrast (DIC). To collect the luminescence of the UCNPs, the sample was excited at 980 nm using the Vision II Ti:Sapphire laser with the emission collected with two non-

descanned GaAsP detectors. The luminescence was measured in the green (550 ± 42.5 nm) and red (655 ± 20 nm) channels.

Incubation of SK-BR-3 cells with propidium iodide

Propidium iodide (5 µL, 1 mg·mL^{-1} in PBS) was mixed with HBSS-based imaging medium (1 mL). The solution was directly added to the coverslip that had been previously placed in a Ludin chamber for imaging (Life Imaging Service, Olten, Switzerland) and incubated at 37 °C in the dark on a heated stage of a Carl Zeiss LSM 510 META microscope for *ca.* 5 min.

Imaging of treated SK-BR-3 cells using a laser scanning confocal microscope

For imaging, 18 mm coverslips containing the SK-BR-3 cells were placed in a Ludin chamber, which was securely tightened. Each coverslip was washed three times with HBSS-based imaging medium and the Ludin chamber was mounted on a heated stage at 37 °C in a Carl Zeiss LSM 510 META microscope. A 543 nm HeNe laser was used to excite either the RB on the surface of the UCNPs or the propidium iodide with the emission collected between 560 – 615 nm in the red channel. DIC images were collected together with fluorescence images. DIC images were recorded with transmitted light at 488 nm using an argon-ion laser.

CellTiter-Blue® cell viability assay

For the viability assays, SK-BR-3 cells were seeded on two 96-well white-bottom microplates *ca.* 48 h prior to treating the cells. The cells were cultured at 37 °C in a 5% CO_2 atmosphere in a 75 cm^2 tissue culture flask until they reached near confluence. At this point, the cells were washed with PBS and harvested from the flask using trypsin 0.25% (1x) EDTA as described previously. The cells were counted with a Neubauer haemocytometer and seeded at a density of 20x10^4 cells/mL (100 µL/well). The cells were incubated at 37 °C in a 5% CO_2 atmosphere for *ca.* 48 h. Following incubation, the cells were washed once with PBS (100 µL). The RB-lysine functionalised NaYF$_4$:Yb,Er,Gd@NaYF$_4$ core-shell UCNPs (50 µL), at concentrations ranging between 10 – 20 µg·mL^{-1}, in McCOY's 5A phenol red free medium containing 0.25% DMSO were added to the wells. Cells without nanoparticles loaded were used as a control. A positive control for cytotoxicity, consisting of a solution of staurosporine (1 mM in DMSO) dispersed in McCOY's 5A phenol red free medium (50 µL; 20 µM), was also used. A control for the effect of DMSO was also performed by treating the cells on the well with McCOY's 5A phenol red free medium containing 0.25% DMSO. The cells were incubated with the UCNPs or the corresponding controls for 3 h at 37 °C in a 5% CO_2 atmosphere. Following incubation, the cells were washed three times with PBS (100 µL) and kept in McCOY's 5A phenol red free medium supplemented with 10% foetal bovine serum (100 µL). One of the 96-well microplates was irradiated using the 980 nm NIR

laser (200 mW, Picotronic) for 6 min per well. The laser was located 50 mm above the 96-well microplate. The other 96 well microplate, which was not irradiated, was covered in aluminium foil in the dark. Following irradiation (and non-irradiation), the cells were further incubated for *ca.* 48 h at 37 °C in a 5% CO_2 atmosphere. CellTiter-Blue® reagent (20 μL) was added to each well and incubated with the cells for 4 h at 37 °C in a 5% CO_2 atmosphere. The fluorescence emission of the CellTiter-Blue® reagent was then measured at 594 nm following excitation at 561 nm using a CLARIOstar® (BMG Labtech) microplate reader. Background fluorescence was corrected by subtracting fluorescence emission from McCOY's 5A phenol red free medium. Cell viability was calculated as a percentage of non-treated, non-irradiated cells. All of the samples were analysed in triplicate.

Results and discussion

Synthesis and characterisation of oleate-capped NaYF$_4$:Yb,Er,Gd@NaYF$_4$ core-shell upconverting nanoparticles

The aim of the research here presented was to synthesise small, highly luminescent nanoparticles that could be readily uptaken by cells for PDT of cancer. Monodisperse β-NaYF$_4$ nanoparticles doped with Yb^{3+}, Gd^{3+} and Er^{3+} (β-NaYF$_4$:Yb,Er,Gd core upconverting nanoparticles) were synthesised as the core material in high temperature boiling solvents following an Ostwald ripening strategy.[6] The size of the core-nanoparticles was determined by TEM. Analysis of the TEM images indicated that the synthesised core UCNPs had a uniform shape and an average diameter of 16.2 ± 0.6 nm (**Fig. S1**). To achieve upconverting nanoparticles with an enhanced luminescence intensity, an inert shell was grown around the core nanoparticles. Cubic α-NaYF$_4$ upconverting nanoparticles with a size of 2 – 3 nm (**Fig. S2**) were synthesised and used as shell precursors. The α-NaYF$_4$ upconverting nanoparticles were injected stepwise to a solution of β-NaYF$_4$:Yb,Er,Gd core UCNPs that was kept at 325 °C. After injection to the core particles, the cubic α-NaYF$_4$ UCNPs dissolved and deposited in a hexagonal crystal lattice on the core UCNPs resulting in the oleate-capped NaYF$_4$:Yb,Er,Gd@NaYF$_4$ core-shell UCNPs.[37] As expected, following addition of the shell material to the core nanoparticles, the size of the nanoparticles increased, as shown by the TEM images, from 16.2 ± 0.6 nm (**Fig. S1**, β-NaYF$_4$:Yb,Er,Gd core UCNPs) to 17.2 ± 1.0 nm (**Fig. 2**, NaYF$_4$:Yb,Er,Gd@NaYF$_4$ core-shell UCNPs). DLS measurements of both core and core-shell UCNPs also indicated an increase in the solvodynamic diameter, from 17.8 ± 2.6 nm to 21.1 ± 3.1 nm, following formation of the shell (**Fig. S3**). The analysis of the composition of the core and core-shell nanoparticles by ICP-OES showed an increase in the Y^{3+} content concomitant with a decrease of the other Ln^{3+} ions from core to core-shell nanoparticles (**Table S1**).
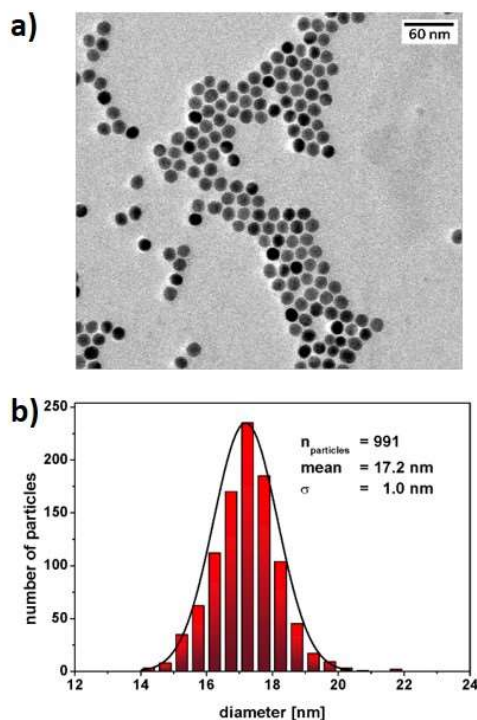
Fig. 2. a) Transmission electron micrograph of a sample of oleate-capped NaYF$_4$:Yb,Er,Gd@NaYF$_4$ core-shell nanoparticles where the scale bar represents 60 nm. **b)** Histogram of the particle size distribution of oleate-capped NaYF$_4$:Yb,Er,Gd@NaYF$_4$ core-shell nanoparticles with an average size of 17.2 ± 1.0 nm (n = 991).

The luminescence spectrum of the β-NaYF$_4$:Yb,Er,Gd core UCNPs recorded following NIR excitation at 980 nm exhibited two main anti-Stokes emission bands subsequently referred to as the green emission ($^4S_{3/2} \rightarrow {}^4I_{15/2}$) at 541 nm and the red emission ($^4F_{9/2} \rightarrow {}^4I_{15/2}$) at 652 nm (**Fig. 3a – i**). The luminescence spectrum of the oleate-capped NaYF$_4$:Yb,Er,Gd@NaYF$_4$ core-shell UCNPs following excitation at 980 nm exhibited also the green and red emission bands at 541 nm and 652 nm, respectively (**Fig. 3a – ii**). A comparison of the luminescence intensities of the core and core-shell nanoparticles following NIR irradiation at 980 nm shows an increase by a factor of 10 when the shell was present. The inactive inert shell minimises surface defects and solvent quenching effects.[34, 38] To achieve high-energy transfer efficiency, a short distance should separate the emitting ions in the UCNPs from the photosensitiser. The short separation distance was achieved by depositing a lysine shell of small *ca.* 1 nm thickness.
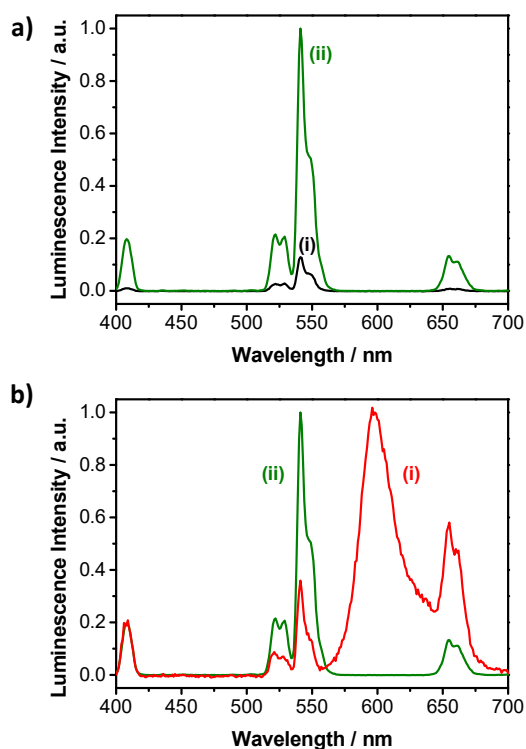
Fig. 3. Luminescence spectra of the **a) (i)** oleate capped β-NaYF$_4$:Yb,Er,Gd core nanoparticles and **(ii)** NaYF$_4$:Yb,Er,Gd@NaYF$_4$ core-shell nanoparticles and **b) (i)** RB-lysine functionalised NaYF$_4$:Yb,Er,Gd@NaYF$_4$ core-shell nanoparticles and **(ii)** NaYF$_4$:Yb,Er,Gd@NaYF$_4$ core-shell nanoparticles. The spectra were recorded in cyclohexane (**a (i and ii)** and **b (ii)**) and DMSO (**b (i)**) following excitation at 980 nm (cw 200 mW). In **a)** the spectra were normalised by the Yb^{3+} concentration determined by ICP-OES, to equal numbers of particles per sample.

Synthesis and characterisation of the RB–lysine functionalised NaYF$_4$:Yb,Er,Gd@NaYF$_4$ core-shell upconverting nanoparticles

Once the highly luminescent oleate-capped NaYF$_4$:Yb,Er,Gd@NaYF$_4$ core-shell UCNPs had been synthesised, the next step was their functionalisation with a photosensitiser to yield a platform that could be used for PDT of breast cancer cells. Rose Bengal (RB) was the chosen photosensitiser since its absorption spectrum overlaps the green luminescence emission band of the UCNPs at 541 nm. Thus, it was expected that, following excitation at 980 nm, the Rose Bengal would be activated *via* a FRET process to produce singlet oxygen.

Before incorporation of the RB, the surface of the oleate-capped NaYF$_4$:Yb,Er,Gd@NaYF$_4$ core-shell UCNPs was modified *via* a two-step ligand exchange method as indicated in **Fig. S4**. In the first step, NOBF$_4$ was inserted in a two-phase system to remove oleate from the surface of the nanoparticles and to stabilise the uncoated particles. This first step resulted in BF$_4^-$-capped NaYF$_4$:Yb,Er,Gd@NaYF$_4$ core-shell UCNPs. In a second step, the ligand L-lysine was bound to the surface of the nanoparticles yielding lysine-capped NaYF$_4$:Yb,Er,Gd@NaYF$_4$ core-shell UCNPs. Water dispersibility of the nanoparticles was achieved following the incorporation of the lysine ligand.

The photosensitiser RB was bound to the free amine groups of the lysine-capped NaYF$_4$:Yb,Er,Gd@NaYF$_4$ core-shell UCNPs *via* classical EDC/NHS chemistry yielding RB-lysine functionalised NaYF$_4$:Yb,Er,Gd@NaYF$_4$ core-shell UCNPs. During the surface modification, the nanoparticles show no tendency of agglomeration, as confirmed by the DLS measurements (**Fig. S5**). A decrease in the solvodynamic diameter of the nanoparticles was observed when the oleate ligand was replaced by BF$_4^-$ (from *ca.* 21 to *ca.* 14 nm). As expected, the solvodynamic diameter increased to 23.7 ± 8.4 nm following incorporation of the Rose Bengal to the lysine-capped NaYF$_4$:Yb,Er,Gd@NaYF$_4$ nanoparticles. The Rose Bengal loading was estimated to be 160 RB molecules per nanoparticle, which is quite similar to the numbers of emitters in the nanoparticle. The RB-lysine functionalised NaYF$_4$:Yb,Er,Gd@NaYF$_4$ core-shell UCNPs exhibited colloidal stability in DMSO and water, and were stable in phosphate buffer and cell medium which enabled assessment of the nanoparticle performance for intracellular experiments.

The surface architecture of the different types of functionalised nanoparticles was validated by FTIR measurements (**Fig. S6**). The FTIR spectrum of the oleate-capped NaYF$_4$:Yb,Er,Gd@NaYF$_4$ core-shell UCNPs exhibited strong C-H stretching at 2,926 and 2,851 cm^{-1} that disappeared, as expected, following ligand exchange with L-lysine. In addition to the C=O stretching (at 1,558 and 1,457 cm^{-1}), a strong absorption band at 1,655 cm^{-1} attributed to the C-N bending was observed in the FTIR spectrum of the lysine-capped UCNPs. Following incorporation of the Rose Bengal, the band due to the amine bending was reduced and new absorption bands occurred at 1,543, 1,457 and 1,342 cm^{-1} that were attributed to the amide stretching and the C=C stretching of the aromatic rings of the photosensitiser. The C-H bending of the aromatic ring and the C-I bending were visible at 954 cm^{-1} and 700 cm^{-1}, respectively.

Optical properties of the RB–lysine functionalised NaYF$_4$:Yb,Er,Gd@NaYF$_4$ core-shell upconverting nanoparticles

Surface modification affects the luminescence characteristics of the UCNPs upon NIR excitation. The spectrum of the RB-lysine functionalised UCNPs shows the emission of the RB overlapping the typical upconversion luminescence (**Fig. 3b**), accompanied by the change of the predominately visible colour of the excited particles from green to red. The green (541 nm) to red (652 nm) ratio of the luminescence emission intensities of the oleate-capped core- shell UCNPs was 7.7:1 (**Fig. 3b − ii**) following 980 nm irradiation. The green to red ratio, under the same irradiation conditions, decreased to 0.6:1 for the RB-lysine functionalised core-shell UCNPs in DMSO (**Fig. 3b − i**) due to the presence of the photosensitiser Rose Bengal, which absorbs light in the region of *ca.* 550 nm. The luminescence spectra of lysine and RB-lysine functionalised core-shell UCNPs in water are reported in **Fig. S7** exhibiting green to red ratios of 5:1 and 0.5:1, respectively. The appearance of the emission of RB observed in **Fig. 3b - i** can be assigned to two effects: a) the so-called inner filter effect and b) Förster resonance energy transfer (FRET). Time-resolved spectroscopy revealed the FRET mechanism by comparing the lifetime of the two main emission peaks of the UCNPs before and after the attachment of the photosensitiser (**Fig. S8** and **Table S2**). The lifetime of the green donor emission decreased from 216 to 161 µs, yielding a FRET efficiency of 25%. The lifetime of the red emission measured at 656 ± 50 nm, containing the long luminescence lifetime of the UCNPs and the short lifetime of RB, decreased from 342 to 266 µs. The acceptor luminescent lifetime of the RB is in the same range compared to the donor lifetime of the green emission. This demonstrates, by introducing L-lysine as short linker molecule, that the weak binding affinity of RB to the surface of the UCNPs was overcome and the distance of the acceptor and donor system was kept as short as possible to enable efficient FRET.

Singlet oxygen production by the RB-lysine functionalised NaYF$_4$:Yb,Er,Gd@NaYF$_4$ core-shell UCNPs

The ability of the RB-lysine functionalised UCNPs to produce singlet oxygen ($^1O_2$) following NIR excitation at 980 nm was investigated using the singlet oxygen probe 9,10-anthracenediyl-bis(methylene) dimalonic acid (ABMA). ABMA is photobleached in the presence of $^1O_2$ and thus the fluorescence emission of the probe is quenched upon reaction with $^1O_2$. The production of $^1O_2$ by the RB-lysine functionalised UCNPs was investigated in two different media: DMSO and McCOY's 5A cell culture medium (**Fig. 4**).

In DMSO, the fluorescence emission intensity of ABMA was readily quenched over time (**Fig. 4a and b – black**) confirming the production of singlet oxygen by the RB photosensitiser on the surface of the UCNPs following NIR excitation at 980 nm. These results confirm the energy transfer between the UCNPs and the photosensitiser and the subsequent production of singlet oxygen. In cell culture medium, the production of singlet oxygen following irradiation of the RB-lysine UCNPs at 980 nm was significantly reduced (**Fig. 4b – red**) due to the quenching of the $^1O_2$ and the absorption of the 980 nm light in the aqueous based medium. Further experiments demonstrate the importance of the short distance between the UCNPs and the photosensitiser for the production of singlet oxygen (**Fig. S9**). The singlet oxygen production of RB-lysine functionalised UCNPs in water was compared to that of lysine functionalised UCNPs in a solution containing dissolved RB. The comparison was performed in two solvents, DMSO and water. When the UCNPs were dispersed in an organic solvent like DMSO, both types of solutions produced more singlet oxygen than the reference system, RB-lysine functionalised UCNPs in water. These results suggest that the distance between the photosensitiser and the UCNPs is not relevant for the production of singlet oxygen in DMSO. The inner filter effect is sufficient to generate singlet oxygen. However, when the experiments were performed in water, production of singlet oxygen was only observed for RB-lysine functionalised UCNPs and not when the RB was in solution and non-covalently attached to the UCNPs. The results obtained in the aqueous media confirm that efficient energy transfer (FRET) is responsible for the production of singlet oxygen by the RB-lysine functionalised UCNPs.
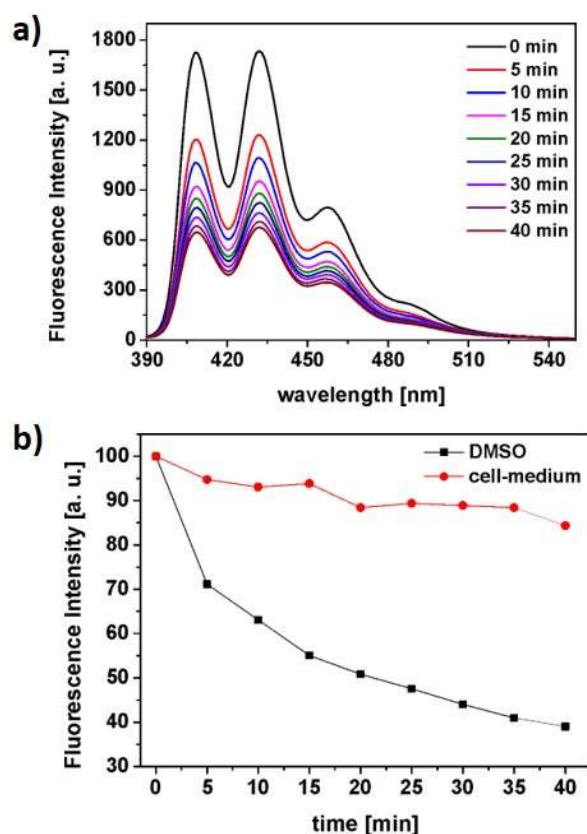
Fig. 4. a) Time-dependent decay of the fluorescence emission spectrum of the singlet oxygen probe 9,10-anthracenediyl-bis(methylene)dimalonic acid (ABMA, λ_{exc} = 380 nm) upon irradiation of the RB-lysine functionalised UCNPs with the NIR-laser (980 nm, cw, 200 mW, DMSO). **b)** Normalised decay of the fluorescence emission intensity of ABMA at 410 nm following irradiation of RB-lysine functionalised UCNPs in DMSO (black) and in McCOY's 5A phenol red free cell culture medium (red).

Cellular uptake of the RB-lysine functionalised NaYF$_4$:Yb,Er,Gd@NaYF$_4$ core-shell UCNPs

The suitability of the RB-lysine functionalised UCNPs to act as PDT agents was studied intracellularly. The first step was to confirm the cellular uptake of the functionalised nanoparticles by SK-BR-3 human breast adenocarcinoma cells. SK-BR-3 cells were incubated with the RB-lysine modified UCNPs for 3 h and the internalisation of the nanoparticles by the cells was investigated using two imaging techniques, *viz*, multi-photon and laser scanning confocal microscopy. To confirm the internalisation of the RB-lysine functionalised UCNPs within the breast cancer SK-BR-3 cells using a multi-photon microscope, the samples were excited using two-photon excitation at two wavelengths: 1) 880 nm to excite the RB on the functionalised UCNPs and to collect the differential interference contrast (DIC) images (**Fig. 5a – c** and **g – i**); and 2) 980 nm to excite the UCNPs directly (**Fig. 5d – f** and **j – l**). Following

two-photon excitation at 880 nm, the fluorescence emission due to the RB on the UCNPs was observed in the green channel (550 ± 42.5 nm; **Fig. 5b**). This emission was not observed in control cells without the RB-lysine functionalised UCNPs loaded (**Fig. 5h**), confirming the presence of the photosensitiser within the SK-BR-3 cells treated with the RB-lysine functionalised UCNPs. No fluorescence emission was observed in the red channel (655 ± 20 nm) following 880 nm irradiation for the cells treated with the functionalised UCNPs (**Fig. 5c**) or for the control cells without UCNPs (**Fig. 5i**). This indicates that the fluorescence observed in the green channel for cells treated with the RB-lysine functionalised UCNPs was due to the RB on the particles. Following 980 nm irradiation, the direct luminescence from the functionalised UCNPs was observed in both the green and in the red channels (**Fig. 5e** and **f**, respectively) as expected from the luminescence spectrum of the UCNPs. This result confirms the uptake of the RB functionalised UCNPs by the SK-BR-3 cells. The upconversion luminescence images of the RB-lysine functionalised UCNPs within the SK-BR-3 cells (**Fig. 5e** and **f**) appeared to be 'blurred' and of poor resolution. Low resolution images of UCNPs obtained using two-photon laser scanning microscopy have been previously reported and are associated with the presence of axial interferences from out-of-focus light together with lateral interferences from scattering within the focal plane. The quality of the upconversion luminescence images could be improved using a microscope equipped with a confocal pinhole, which would eliminate both the axial and lateral interferences.[39] Despite the blurred images (**Fig. 5e** and **f**), it is clear that the RB-lysine functionalised UCNPs are successfully emitting upconversion luminescence from within the cancer cells. No upconversion luminescence was observed when control cells with no RB-lysine functionalised UCNPs were imaged following irradiation using the 980 nm NIR laser under the same conditions (**Fig. 5k** and **l**).
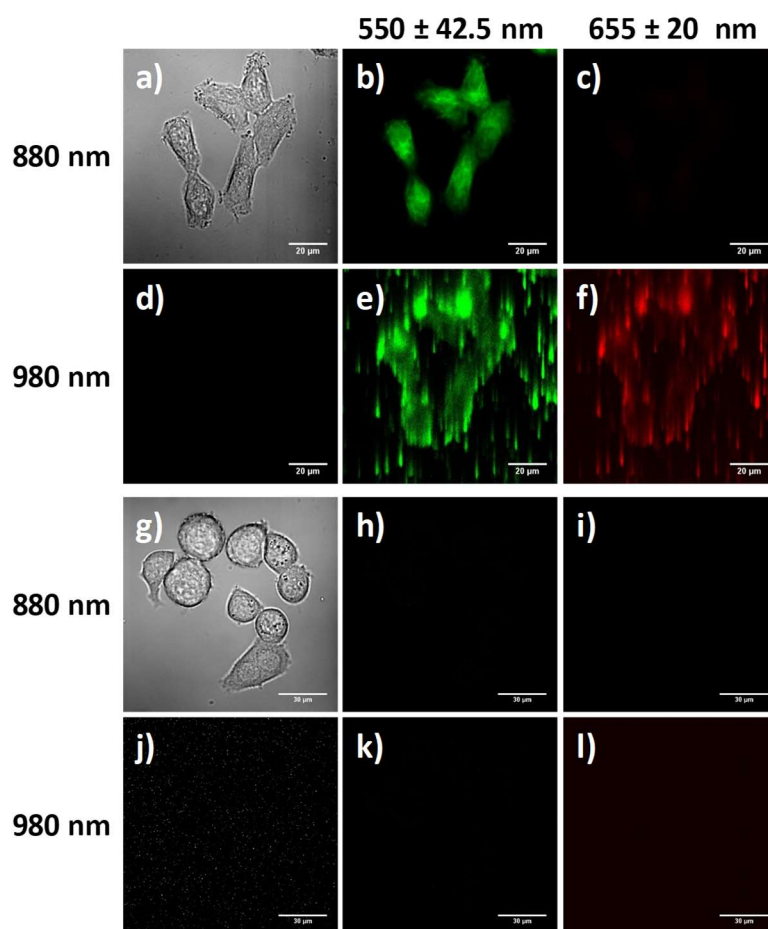
Fig. 5. Multi-photon microscopy images of SK-BR-3 cells: **a – f)** incubated with RB-lysine functionalised UCNPs (25 µg·mL^{-1}) and **g – l)** control cells without functionalised UCNPs. DIC images were obtained using an 880 nm laser (**a** and **g**). The emission was collected in the green (550 ± 42.5 nm; **b, e, h** and **k**) and red (655 ± 20 nm; **c, f, i** and **l**) channels following excitation at either 880 or 980 nm. Scale bars: **a – f)** 20 µm and **g – l)** 30 µm.

The experiments performed using the confocal microscope also confirmed the internalisation of the RB functionalised UCNPs within the SK-BR-3 cells. The cells were incubated with the RB-lysine functionalised UCNPs for 3 h and the emission due to the RB on the nanoparticles was collected in the red channel (560 – 615 nm) following excitation with a 543 nm HeNe laser (**Fig. 6a - c**). The morphology of the treated cells was observed in the DIC images obtained with transmitted light at 488 nm. Laser scanning confocal microscopy images of the treated cells (**Fig. 6a – c**) show an intense red emission due to the RB of the functionalised UCNPs within the cells that was not observed in control cells (**Fig. 6d – f**). Morphological changes were not observed for either of the cell samples suggesting that the RB-lysine UCNPs were not toxic to the cells.
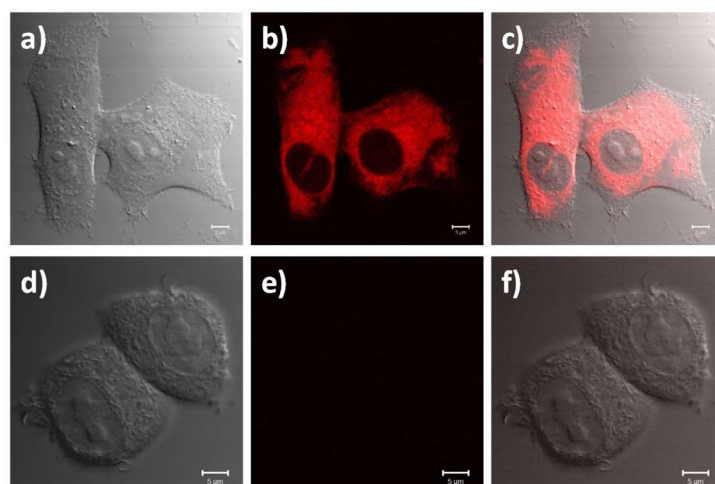
Fig. 6. Laser scanning confocal microscopy images of SK-BR-3 cells: **a – c)** incubated with RB-lysine functionalised UCNPs (25 µg·mL^{-1}) and **d – f)** control cells without functionalised UCNPs. DIC images were obtained using a 488 nm laser (**a** and **d**). The emission due to the RB on the UCNPs was collected in the red channel (560 – 615 nm; **b** and **e**) following excitation at 543 nm. Images **c** and **f** are composite images of the DIC and red channels. Scale bars are 5 µm.

Suitability of the RB-lysine functionalised NaYF$_4$:Yb,Er,Gd@NaYF$_4$ UCNPs for photodynamic therapy of breast cancer cells

To establish the efficacy of the functionalised UCNPs as PDT agents, a CellTiter-Blue® cell viability assay[40] was performed *in vitro*. This assay provides information regarding the number of viable cells present in the wells of a 96-well plate by measuring the metabolic capacity of the studied cells. Viable cells are able to reduce the indicator dye resazurin into a fluorescent product, resorufin, the fluorescence emission intensity of which can be measured at 594 nm using a microplate reader upon excitation at 561 nm. Conversely, non-viable cells lose their metabolic capacity and are not able to reduce resazurin thus are unable to generate a measurable fluorescent signal. SK-BR-3 cells were seeded on 96-well microplates and incubated with varying concentrations of RB-lysine functionalised UCNPs for 3 h. A positive control for cytotoxicity, consisting of cells treated with staurosporine, was also included in the assay. Following incubation with the RB-lysine functionalised UCNPs, the cells were thoroughly washed with PBS to remove the nanoparticles that had not been internalised by the SK-BR-3 cells. The cells were subjected to PDT by irradiation with a NIR 980 nm laser for 6 min per well.

Control experiments where cells incubated with the varying concentrations of RB-lysine functionalised UCNPs and with staurosporine were kept in the dark and not irradiated were also performed. Cell

20

viability of the SK-BR-3 cells was assessed 48 h following PDT treatment (**Fig. 7**). A decrease in cell viability concomitant with an increase in the concentration of RB-lysine functionalised UCNPs (from 0 to 20 μg·mL^{-1}) can be observed following PDT treatment of the SK-BR-3 cells. However, at high concentrations *(i.e. $\geq$ 20 μg·mL^{-1})* the nanoparticles exhibited some dark toxicity as indicated by the decrease in viability of cells that had been incubated with the functionalised UCNPs but had not been irradiated. At a concentration of functionalised UCNPs of 15 μg·mL^{-1}, 67% of the cells were killed following PDT while the dark toxicity of the nanoparticles was minimal (5%). The effect that the DMSO used to solubilise the functionalised UCNPs had on the viability of the cells was also investigated. No cell-death was observed when the SK-BR-3 cells were treated with McCOY's 5A phenol red free medium containing 0.25% DMSO for 3 h confirming that, under the conditions used to perform the cell viability assay, DMSO was not toxic for the cells. The results from the CellTiter-Blue® cell viability assay suggested that a concentration of 15 μg·mL^{-1} of the RB-lysine functionalised UCNPs was ideal for PDT.
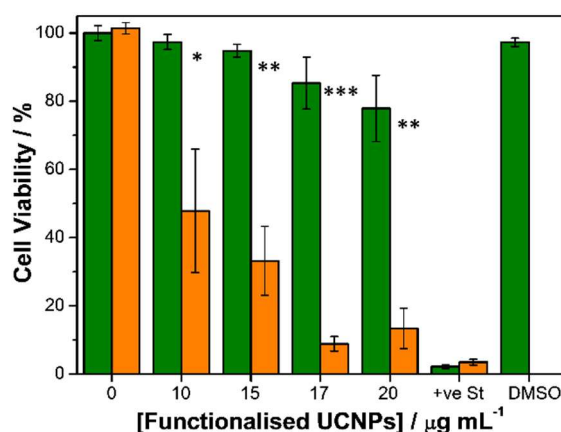

Fig. 7. CellTiter-Blue® cell viability assay of SK-BR-3 cells that were incubated with varying concentrations (from 0 to 20 μg·mL^{-1}) of RB-lysine functionalised UCNPs for 3 h and irradiated (orange) or non-irradiated (green) with the 980 nm NIR laser for 6 min. +ve St indicates SK-BR-3 cells that had been treated with staurosporine – a positive control for cytotoxicity. DMSO indicates SK-BR-3 cells that had been treated with McCOY's 5A phenol red free medium containing 0.25% DMSO for 3 h. Each experiment was repeated in triplicate and the relative standard error is indicated by the error bars. Statistically significant difference between non-irradiated and irradiated samples is indicated by * at $P < 0.04$; ** at $P < 0.0006$ and *** at $P < 0.00007$, obtained using a two-tailed Student's t-test, where $P < 0.05$ is considered statistically significant.

Laser scanning confocal fluorescence microscopy was used to further determine the suitability of the functionalised UCNPs for PDT. SK-BR-3 cells seeded on coverslips were treated with the RB-lysine functionalised UCNPs (15 μg·mL^{-1}) for 3 h. Following removal of non-uptaken nanoparticles by washing, singlet oxygen was activated by irradiating the UCNPs within the cells with the 980 nm NIR laser for 6 min. The treated cells were imaged using confocal laser scanning microscopy *ca.* 24 h following PDT treatment (**Fig. 8a – c**). DIC images of the SK-BR-3 cells clearly show degradation of the cell membrane, which was indicative of cell death (**Fig. 8a** and **d**). The RB-lysine functionalised UCNPs accumulated in the nucleus of the SK-BR-3 cells that had been irradiated with the 980 nm NIR laser (**Fig. 8b** and **c**). The accumulation of the particles in the nucleus of the cells was not observed for non-irradiated SK-BR-3 cells that had been incubated with the RB-lysine functionalised UCNPs (**Fig. 8j – l** and **Fig. S10**). This result suggests that the location of the UCNPs in the nucleus, seen in **Fig. 8b** and **c**, following NIR PDT could be indicative of cell death. Furthermore, the cells that had been treated with the RB-lysine functionalised UCNPs and irradiated with the 980 nm NIR laser subsequently stained positive when incubated with propidium iodide (**Fig. 8d – f** and **Fig. S11**) confirming the cell death following PDT treatment.[41]
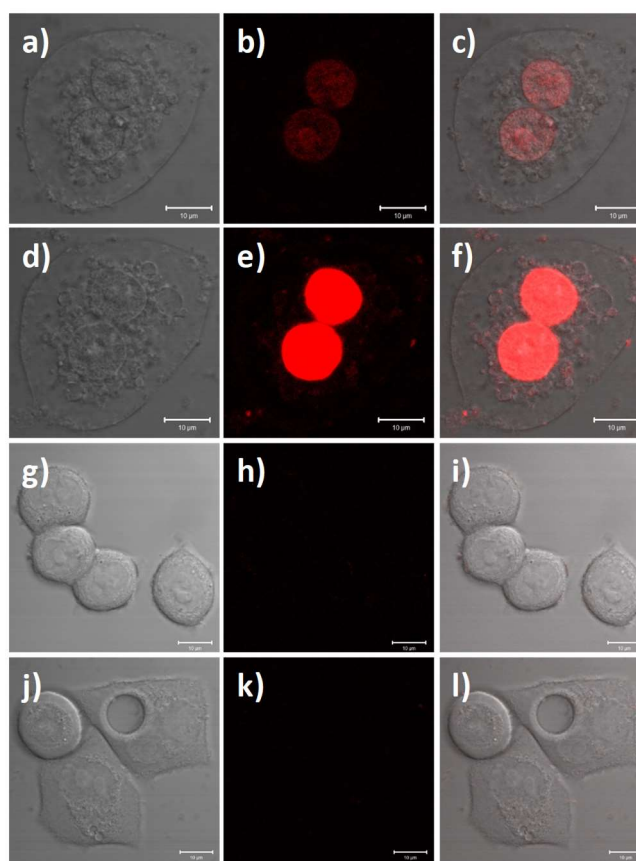
Fig. 8. Laser scanning confocal microscopy images of SK-BR-3 cells: **a − f)** incubated with the RB-lysine functionalised UCNPs (15 µg·mL^{-1}) and irradiated with the 980 nm laser before (**a − c**) and following (**d − f**) addition of propidium iodide; **g − i)** without RB-lysine functionalised UCNPs, irradiated with the 980 nm laser and treated with propidium iodide; and **j − l)** incubated with the RB-lysine functionalised UCNPs (15 µg·mL^{-1}), non-irradiated with the 980 nm laser and treated with propidium iodide. DIC images were obtained using a 488 nm laser (**a, d, g** and **j**). The fluorescence emission due to the RB on the UCNPs and the propidium iodide was collected in the red channel (560 − 615 nm; **b, e, h** and **k**) following excitation at 543 nm (laser power 4%). Images **c, f, i** and **l** are composite images of the red and DIC channels. Scale bars are 10 µm.

The changes of cellular membrane integrity or the positive stain for propidium iodide were not observed for the control experiments. These included: the SK-BR-3 cells without functionalised UCNPs that had been irradiated with the 980 nm NIR laser for 6 min (**Fig. 8g − i**); the non-irradiated SK-BR-3 cells incubated with the functionalised UCNPs (**Fig. 8j − l**); and the non-irradiated SK-BR-3 cells without functionalised UCNPs (**Fig. S12**). The laser power used to image the SK-BR-3 cells treated with propidium iodide was too low (4%) to be able to observe the fluorescence emission due to the internalised RB-lysine functionalised UCNPs in the non-irradiated SK-BR-3 cells shown in **Fig. 8j − l**. To confirm the presence of the RB-lysine functionalised UCNPs in the non-irradiated SK-BR-3 cells, images

23

using a higher laser power (100%) were obtained prior to the addition of the propidium iodide and compared with the control non-irradiated SK-BR-3 cells without RB-lysine functionalised UCNPs imaged under the same conditions (**Fig. S10**). The fluorescence emission due to the RB from the SK-BR-3 cells that had been treated with the RB-lysine functionalised UCNPs was not observed for the control cells, thus confirming the internalisation of the RB-lysine functionalised UCNPs by the SK-BR-3 cells and the importance of NIR 980 nm irradiation to induce cell death *via* PDT. The results shown in **Fig. 8** and **Fig. S10 – S12** highlight that the RB-lysine functionalised UCNPs are ideal photosensitiser vehicles for PDT of breast cancer cells.

Conclusions

Highly luminescent lanthanide doped core-shell upconverting nanoparticles have been synthesised and functionalised with the photosensitiser Rose Bengal *via* an amino acid (L-lysine) linker. The short distance between the photosensitiser and the light emitting core has proven efficient for a high energy transfer from the UCNPs core to the RB *via* a FRET process. The FRET process, confirmed from luminescence lifetime measurements, allowed for the excitation of the photosensitiser and thus the production of singlet oxygen using NIR light at 980 nm. The RB-lysine functionalised UCNPs were successfully used for PDT of SK-BR-3 breast cancer cells. The efficient internalisation of the RB-lysine functionalised UCNPs by the cells was confirmed using confocal laser scanning microscopy and multi-photon microscopy, which clearly showed the emission from both the RB and the UCNPs only inside the treated cells. Following internalisation of the functionalised UCNPs, the SK-BR-3 cells were irradiated with a 980 nm laser to induce the production of singlet oxygen by RB. Cell viability assays showed high levels of cell death following irradiation, reaching *ca.* 67% of cell death at a RB-lysine functionalised UCNP concentration of only 15 μg$\cdot$mL^{-1}. Additionally, at this concentration, the RB-lysine functionalised UCNPs were shown to induce negligible dark toxicity of the SK-BR-3 cells that had not been irradiated. The efficient cell death post-PDT was also confirmed using confocal microscopy and the dead cell marker propidium iodide. Only those cells that had been incubated with the RB-lysine functionalised UCNPs and irradiated with NIR light at 980 nm stained positive with propidium iodide, thus confirming the cell death following PDT treatment. The confocal microscopy experiments also showed accumulation of the UCNPs in the nucleus of the SK-BR-3 cells, only in samples that had been irradiated with NIR light to induce production of singlet oxygen. Control cells, treated with the functionalised nanoparticles but not irradiated, did not show accumulation of the UCNPs within the nucleus. For future applications, targeting agents could be incorporated onto the surface of the nanoparticles yielding a vehicle for targeted photodynamic therapy to further improve the efficiency

24

of the treatment and reduce any possible damage of healthy cells. Furthermore, to complement the treatment potential of the nanoplatform, the nanocrystals doped with Gd^{3+} can also be used as a multimodal diagnostic tool for magnetic resonance imaging (MRI).

The synthesised efficient RB-lysine functionalised UCNPs are shown to be successful candidates for PDT of breast cancer cells using NIR light. The NIR irradiation opens the possibility to use the reported nanoplatform to treat deep lying tumours.

Conflicts of interest

There are no conflicts to declare.

Acknowledgements

Bibliographic references and notes

1. J. P. Celli, B. Q. Spring, I. Rizvi, C. L. Evans, K. S. Samkoe, S. Verma, B. W. Pogue and T. Hasan, Imaging and photodynamic therapy: mechanisms, monitoring, and optimization, *Chem. Rev.*, 2010, **110**, 2795-2838.
2. K. Plaetzer, B. Krammer, J. Berlanda, F. Berr and T. Kiesslich, Photophysics and photochemistry of photodynamic therapy: fundamental aspects, *Laser Med. Sci.*, 2009, **24**, 259-268.
3. P. García Calavia, M. J. Marín, I. Chambrier, M. J. Cook and D. A. Russell, Towards optimisation of surface enhanced photodynamic therapy of breast cancer cells using gold nanoparticle-photosensitiser conjugates, *Photochem. Photobiol. Sci.*, 2018, **17**, 281-289.
4. G. Obaid, I. Chambrier, M. J. Cook and D. A. Russell, Targeting the oncofetal Thomsen–Friedenreich disaccharide using Jacalin-PEG phthalocyanine gold nanoparticles for photodynamic cancer therapy. *Angew. Chem., Int. Ed.*, 2012 **51**, 6158-6162.
5. M. J. Marín and D. A. Russell, *Near-infrared nanomaterials: preparation, bioimaging and therapy applications*, ed. F. Zhang, Royal Society of Chemistry, Cambridge, U. K., 2016, Chapter 7, pp. 192-231.

6. G. Chen, H. Qiu, P. N. Prasad and X. Chen, Upconversion nanoparticles: design, nanochemistry, and applications in theranostics, *Chem. Rev.*, 2014, **114**, 5161-5214.

7. M. Wang, G. Abbineni, A. Clevenger, C. B. Mao and S. K. Xu, Upconversion nanoparticles: synthesis, surface modification and biological applications, *Nanomed. Nanotechnol. Biol. Med.*, 2011, **7**, 710-729.

8. S. Jiang, M. K. Gnanasammandhan and Y. Zhang, Optical imaging-guided cancer therapy with fluorescent nanoparticles, *J. Royal Soc. Interface*, 2010, **7**, 3-18.

9. M. Haase and H. Schäfer, Upconverting nanoparticles. *Angew. Chem., Int. Ed.*, 2011, **50**, 5808-5829.

10. J. F. Suyver, J. Grimm, M. K. van Veen, D. Biner, K. W. Kramer and H. U. Gudel, Upconversion spectroscopy and properties of $NaYF_4$ doped with Er ($^{3+}$), Tm^{3+} and/or Yb^{3+}, *J. Lumin.*, 2006, **117**, 1-12.

11. A. G. Arguinzoniz, E. Ruggiero, A. Habtemariam, J. Hernández-Gil, L. Salassa and J. C. Mareque-Rivas, Light harvesting and photoemission by nanoparticles for photodynamic therapy, *Part. Part. Syst. Char.*, 2014, **31**, 46-75.

12. S. Wilhelm, T. Hirsch, W. M. Patterson, E. Scheucher, T. Mayr and O. S. Wolfbeis, Multicolor upconversion nanoparticles for protein conjugation, *Theranostics*, 2013, **3**, 239-248.

13. V. Muhr, S. Wilhelm, T. Hirsch and O. S. Wolfbeis, Upconversion nanoparticles: from hydrophobic to hydrophilic surfaces. *Acc. Chem. Res.*, 2014, **47**, 3481-3493.

14. C. Wang, L. Cheng and Z. Liu, Upconversion nanoparticles for photodynamic therapy and other cancer therapeutics, *Theranostics*, 2013, **3**, 317-330.

15. P. Zhang, W. Steelant, M. Kumar and M. Scholfield, Versatile photosensitizers for photodynamic therapy at infrared excitation, *J. Am. Chem. Soc.*, 2007, **129**, 4526-4527.

16. Y. Guo, M. Kumar and P. Zhang, Nanoparticle-based photosensitizers under CW infrared excitation, *Chem. Mater.*, 2007, **19**, 6071-6072.

17. X. Yang, Q. Xiao, C. Niu, N. Jin, J. Ouyang, X. Xiao and D. He, Multifunctional core-shell upconversion nanoparticles for targeted tumor cells induced by near-infrared light, *J. Mater. Chem. B*, 2013, **1**, 2757-2763.

18. H. Guo, H. Qian, N. M. Idris and Y. Zhang, Singlet oxygen-induced apoptosis of cancer cells using upconversion fluorescent nanoparticles as a carrier of photosensitizer, *Nanomed. Nanotechnol. Biol. Med.*, 2010, **6**, 486-495.

19. H. S. Qian, H. C. Guo, P. C. -L. Ho,R. Mahendran, and Y. Zhang, Mesoporous-silica-coated up-conversion fluorescent nanoparticles for photodynamic therapy, *Small*, 2009, **5**, 2285-2290.

20. B. B. Hou, B. Zheng, X. Q. Gong, H. J. Wang, S. Wang, Z. Y. Liao, X. D. Li, X. N. Zhang and J. Chang, A UCN@mSiO(2)@cross-linked lipid with high steric stability as a NIR remote controlled-release nanocarrier for photodynamic therapy, *J. Mater. Chem. B*, 2015, **3**, 3531-3540.

21. M. Gonzalez-Bejar, M. Liras, L. Frances-Soriano, V. Voliani, V. Herranz-Perez, M. Duran-Moreno, J. M. Garcia-Verdugo, E. I. Alarcon, J. C. Scaiano and J. Perez-Prieto, NIR excitation of upconversion nanohybrids containing a surface grafted Bodipy induces oxygen-mediated cancer cell death, *J. Mater. Chem. B*, 2014, **2**, 4554-4563.

22. J. Shan, S. J. Budijono, G. Hu, N. Yao, Y. Kang, Y. Ju and R. K. Prud'homme, Pegylated composite nanoparticles containing upconverting phosphors and meso-tetraphenyl porphine (TPP) for photodynamic therapy, *Adv. Funct. Mater.*, 2011, **21**, 2488-2495.

23. C. Wang, H. Tao, L. Cheng and Z. Liu, Near-infrared light induced in vivo photodynamic therapy of cancer based on upconversion nanoparticles, *Biomaterials*, 2011, **32**, 6145-6154.

24. X. Wang, K. Liu, G. Yang, L. Cheng, L. He, Y. Liu, Y. Li, L. Guo and Z. Liu, Near-infrared light triggered photodynamic therapy in combination with gene therapy using upconversion nanoparticles for effective cancer cell killing, *Nanoscale*, 2014, **6**, 9198-9205.

25. S. S. Lucky, N. Muhammad Idris, Z. Li, K. Huang, K. C. Soo and Y. Zhang, Titania coated upconversion nanoparticles for near-infrared light triggered photodynamic therapy, *ACS Nano*, 2015, **9**, 191-205.

26. K. Liu, X. Liu, Q. Zeng, Y. Zhang, L. Tu, T. Liu, X. Kong, Y. Wang, F. Cao, S. A. G. Lambrechts, M. C. G. Aalders and H. Zhang, Covalently Assembled NIR Nanoplatform for Simultaneous Fluorescence Imaging and Photodynamic Therapy of Cancer Cells, *ACS Nano*, 2012, **6**, 4054-4062.

27. D. K. Chatterjee and Y. Zhang, Upconverting nanoparticles as nanotransducers for photodynamic therapy in cancer cells. *Nanomedicine*, 2008, **3**, 73-82.

28. A. Zhou, Y. Wei, B. Wu, Q. Chen and D. Xing, Pyropheophorbide A and c(RGDyK) comodified chitosan-wrapped upconversion nanoparticle for targeted near-infrared photodynamic therapy, *Mol. Pharm.*, 2012, **9**, 1580-1589.

29. S. Cui, H. Chen, H. Zhu, J. Tian, X. Chi, Z. Qian, S. Achilefu and Y. Gu, Amphiphilic chitosan modified upconversion nanoparticles for in vivo photodynamic therapy induced by near-infrared light, *J. Mater. Chem.*, 2012, **22**, 4861-4873.

30. H. Wang, Z. Liu, S. Wang, C. Dong, X. Gong, P. Zhao and J. Chang, MC540 and upconverting nanocrystal coloaded polymeric liposome for near-infrared light-triggered photodynamic therapy and cell fluorescent imaging, *ACS Appl. Mater. Interfaces*, 2014, **6**, 3219-3225.

31. G. Tian, W. Ren, L. Yan, S. Jian, Z. Gu, L. Zhou, S. Jin, W. Yin, S. Li and Y. Zhao, Red-emitting upconverting nanoparticles for photodynamic therapy in cancer cells under near-infrared excitation, *Small*, 2013 **9**, 1929-1938.

32. L. Zhou, Z. Li, Z. Liu, M. Yin, J. Ren and X. Qu, One-step nucleotide-programmed growth of porous upconversion nanoparticles: application to cell labeling and drug delivery, *Nanoscale*, 2014, **6**, 1445-1452.

33. M. Wang, Z. Chen, W. Zheng, H. Zhu, S. Lu, E. Ma, D. Tu, S. Zhou, M. Huang and X. Chen, Lanthanide-doped upconversion nanoparticles electrostatically coupled with photosensitizers for near-infrared-triggered photodynamic therapy, *Nanoscale*, 2014, **6**, 8274-8282.

34. V. Muhr, C. Wurth, M. Kraft, M. Buchner, A. J. Baeumner, U. Resch-Genger and T. Hirsch, Particle-size-dependent forster resonance energy transfer from upconversion nanoparticles to organic dyes, *Anal. Chem.*, 2017, **89**, 4868-4874.

35. S. Wilhelm, M. Kaiser, C. Wurth, J. Heiland, C. Carrillo-Carrion, V. Muhr, O. S. Wolfbeis, W. J. Parak, U. Resch-Genger and T. Hirsch, Water dispersible upconverting nanoparticles: effects of surface modification on their luminescence and colloidal stability, *Nanoscale*, 2015, **7**, 1403-1410.

36. F. Hund, Das ternäre Fluorid NaYF₄. *Zeitschrift für anorganische Chemie*, 1950, **261**, 106-115.

37. N. J. J. Johnson, A. Korinek, C. H. Dong and F. C. J. M. van Veggel, Self-focusing by Ostwald ripening: a strategy for layer-by-layer epitaxial growth on upconverting nanocrystals, *J. Am. Chem. Soc.*, 2012, **134**, 11068-11071.

38. C. Wurth, M. Kaiser, S. Wilhelm, B. Grauel, T. Hirsch and U. Resch-Genger, Excitation power dependent population pathways and absolute quantum yields of upconversion nanoparticles in different solvents, *Nanoscale*, 2017, **9**, 4283-4294.

39. M. Yu, F. Li, Z. Chen, H. Hu, C. Zhan, H. Yang and C. Huang, Laser scanning up-conversion luminescence microscopy for imaging cells labeled with rare-earth nanophosphors, *Anal. Chem.*, 2009, **81**, 930-935.

40. N. P. Gabrielson and D. W. Pack, Acetylation of polyethylenimine enhances gene delivery via weakened polymer/DNA interactions, *Biomacromolecules*, 2006, **7**, 2427-2435.

41. C. Riccardi and I. Nicoletti, Analysis of apoptosis by propidium iodide staining and flow cytometry, *Nat. Protocols*, 2006, **1**, 1458-1461.